International Journal of
*Molecular Sciences*

MDPI

*Article*

# Two Novel Fluorescence Probes Based on Caffeic Acid Derivative for Phosphate Ions and Their Applications in Biological Samples

**Xiaowen Zhou [1], Xiaoqin Yang [1], Xiaoping Rao [2], Yingjun Zhang [3], Ping Zhao [1] and Qian Jiang [1,*]**

[1] Key Laboratory of State Forestry and Grassland Administration on Highly-Efficient Utilization of Forestry Biomass Resources in Southwest China, Southwest Forestry University, Kunming 650224, China; zhouxw0504@outlook.com (X.Z.); yangxiaoqin@swfu.edu.cn (X.Y.); hypzhao@swfu.edu.cn (P.Z.)
[2] College of Chemical Engineering, Huaqiao University, Xiamen 361021, China; raoxp@hqu.edu.cn
[3] Laboratory of Phytochemistry and Plant Resources in West China, Kunming Institute of Botany, Chinese Academy of Sciences, Kunming 650204, China; zhangyj@mail.kib.ac.cn
* Correspondence: qjiang@swfu.edu.cn

**Abstract:** Phosphate is widely used in industry and agriculture fields. However, excess accumulation of $PO_4^{3-}$ causes several adverse effects on the human body and ecological environment. Consequently, it is important to develop a simple method for the detection of $PO_4^{3-}$ concentration in the ecological environment and in vivo. Herein, two caffeic acid derivative-based fluorescence probes (**BAM-HM** and **BAM-HH**) were developed for the detection of phosphate. The **BAM-HM** probe could detect phosphate via fluorescence enhancement at 500 nm, with the detection limit being 0.612 μM. Meanwhile, the **BAM-HH** probe showed a significant turn-on signal at 450 nm after the addition of phosphate, and the detection limit was calculated to be 0.318 μM. The sensing mechanism was determined by $^1$H NMR and MS. Furthermore, the two probes (**BAM-HM** and **BAM-HH**) were applied for $PO_4^{3-}$detection in living cells and water samples.

**Keywords:** fluorescent probe; caffeic acid derivative; highly selective; phosphates; cell imaging

check for updates

**Citation:** Zhou, X.; Yang, X.; Rao, X.; Zhang, Y.; Zhao, P.; Jiang, Q. Two Novel Fluorescence Probes Based on Caffeic Acid Derivative for Phosphate Ions and Their Applications in Biological Samples. *Int. J. Mol. Sci.* **2024**, *25*, 11680. https://doi.org/10.3390/ijms252111680

Academic Editor: Richard H. W. Funk

Received: 24 September 2024
Revised: 16 October 2024
Accepted: 24 October 2024
Published: 30 October 2024

**Copyright:** © 2024 by the authors. Licensee MDPI, Basel, Switzerland. This article is an open access article distributed under the terms and conditions of the Creative Commons Attribution (CC BY) license (https://creativecommons.org/licenses/by/4.0/).

## 1. Introduction

Because of its unique chemical properties, phosphate ($PO_4^{3-}$) plays an important role in many industrial and agricultural fields, such as chemical reagents, fertilizers, foods, pharmaceuticals, and animal feeds [1–3]. In the food industry, phosphate ions are often applied in the production of food additives. As a necessary nutrient element for plant growth, phosphorus is transformed into plant auxin after entering the plant [4,5]. Currently, due to the wide application of phosphate, a large amount of phosphate is released into the aquatic environment and ultimately enters the human body through the food chain [6–8]. Regarding human health, studies have shown that excessive phosphate intake may interfere with the absorption of calcium, lead to an imbalance of calcium and phosphorus, and increase the risk of bone disease [9,10]. In addition, excessive intake of phosphate ions may also burden the kidneys and aggravate pre-existing kidney disease [11]. Therefore, it is essential to determine the changes in phosphate content in biological processes.

To date, several traditional analytical techniques have been developed for the detection of $PO_4^{3-}$, such as liquid or gas chromatography–mass spectrometry, surface-enhanced Raman spectroscopy, high-performance liquid chromatography, and electrochemistry [12–15]. Compared with these traditional detection methods, the fluorescence analysis method can be used as an effective analytical tool because of its advantages, such as high sensitivity and selectivity, convenience, real-time detection, and low cost [16–19]. To date, a large number of fluorescence probes with excellent fluorescent properties for the detection of biomolecules have been designed [20–23]. Among these reported specific fluorescence probes, few fluorescence probes for the detection of phosphate have been reported [24–28].

Therefore, it is still a challenge to design $PO_4^{3-}$ fluorescence probes with high sensitivity and selectivity that can be applied for detection in living cells.

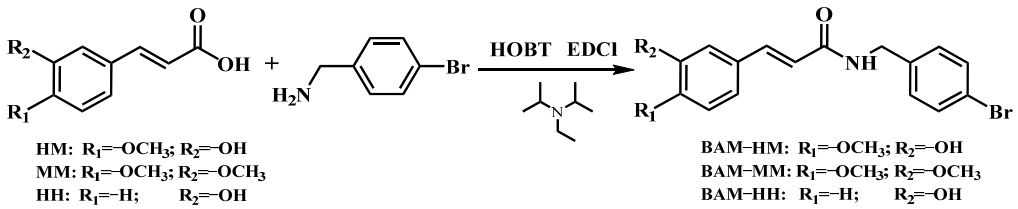
Due to its outstanding pharmacological activities, including antidepressant, antioxidant, and anticancer effects, caffeic acid (CA) is regarded as a bioactive molecule in plants [29–32] and is often employed in the design of drug molecules. Nevertheless, the structure of CA contains one phenyl group and two hydroxyl groups, which is beneficial for the enhancement of fluorescence intensity. Currently, reports of fluorescent probes based on CA are still rare [33]. As a result, developing a unique fluorescent probe based on CA is quite desirable.

Herein, three CA derivatives (**BAM-HM**, **BAM-MM**, and **BAM-HH**) were successfully synthesized. **BAM-HM** and **BAM-HH** could be used as $PO_4^{3-}$ probes. These two $PO_4^{3-}$ probes possess some advantages, such as high selectivity, a low detection limit (**BAM-HM**, 0.612 μM; **BAM-HH**, 0.318 μM), and real-time detection. Furthermore, for practical applications, the **BAM-HM** and **BAM-HH** probes are capable of determining the $PO_4^{3-}$ concentration in living cells and real water.

## 2. Results and Discussion

### *2.1. Synthesis*

In this work, three caffeic acid derivatives were designed and synthesized through a simple synthetic route (Scheme 1). All the final products were purified and characterized by $^1$H NMR, $^{13}$C NMR, and HRMS, which confirmed their molecular structures (Figures S1–S9).




**Scheme 1.** Synthesis route of **BAM-HM**, **BAM-MM** and **BAM-HH**.

### *2.2. Photophysical Properties of **BAM-HM**, **BAM-MM**, and **BAM-HH***

Initially, we studied the photophysical properties of **BAM-HM**, **BAM-MM**, and **BAM-HH**. As shown in Figure 1, the three compounds all displayed weak fluorescence, and the fluorescence quantum yields (φ) of **BAM-HM**, **BAM-MM**, and **BAM-HH** were 0.0231, 0.014, and 0.016. However, in the solution of **BAM-HM**, the addition of $PO_4^{3-}$ triggered a new emission peak at 500 nm, accompanied by green fluorescence (φ = 0.361). In addition, after the addition of $PO_4^{3-}$, the fluorescence emission peak of **BAM-HH** at 450 nm appeared, and obvious blue fluorescence was observed (φ = 0.458). Finally, no significant fluorescence enhancement appeared in the solution of **BAM-MM** + $PO_4^{3-}$ (φ = 0.017). Figure S10 shows the UV–vis spectral changes upon the addition of $PO_4^{3-}$. **BAM-HM**, **BAM-MM,** and **BAM-HH** showed obvious absorption maxima at around 320 nm, 320 nm, and 300 nm, respectively. Then, upon the addition of $PO_4^{3-}$ to the **BAM-MM** compound, no obvious absorption band change appeared in the UV–vis spectra. Surprisingly, upon the addition of $PO_4^{3-}$ to the solutions of **BAM-HM** and **BAM-HH**, both absorption maxima at 320 nm and 300 nm decreased significantly, and two new absorption peaks appeared at 370 nm and 354 nm, respectively. These results indicated that **BAM-HM** and **BAM-HH** could be employed as fluorescence probes for $PO_4^{3-}$ detection.

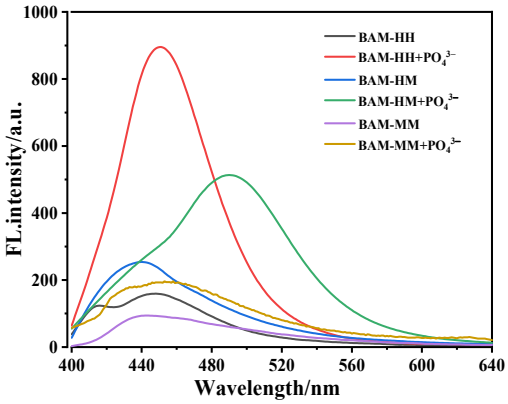



**Figure 1.** Fluorescence spectra of three compounds, **BAM-HM**, **BAM-MM**, and **BAM-HH**, in the presence of $PO_4^{3-}$ in DMF/$H_2O$ (pH = 7.0, 50% DMF).

### *2.3. Spectroscopic Response of Probe **BAM-HM** to $PO_4^{3-}$*

First, the selectivity of the **BAM-HM** probe toward various anions and cations was investigated; as shown in Figures 2A and S11, only $PO_4^{3-}$ led to a significant fluorescence change, and other ions were not found in any variations. Meanwhile, the fluorescence solution of the **BAM-HM** probe changed from colorless to green (Figure 2B). In addition, an obvious fluorescence intensity enhancement at 500 nm was observed after the addition of $PO_4^{3-}$ to the solution of the **BAM-HM** probe.

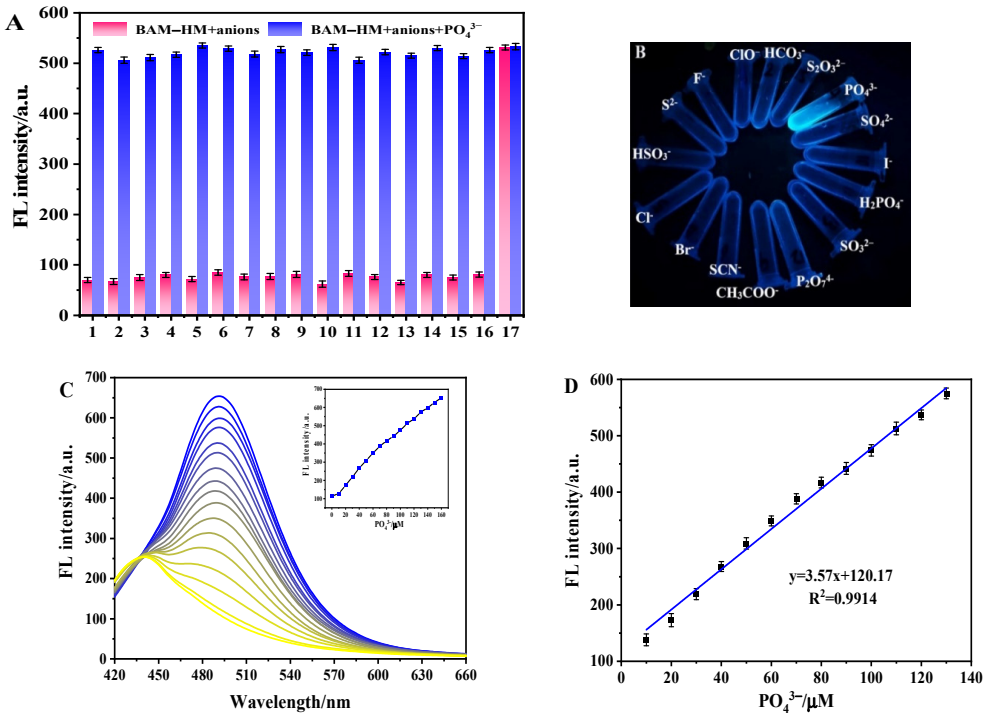



**Figure 2.** (**A**) Selectivity and interference of the **BAM-HM** probe for anions (1–16: $F^-$, $Cl^-$, $Br^-$, $I^-$, $HCO_3^-$, $CO_3^{2-}$, $AcO^-$, $SCN^-$, $SO_3^{2-}$, $ClO^-$, $HSO_3^-$, $SO_4^{2-}$, $S^{2-}$, $S_2O_3^{2-}$, $HPO_4^{2-}$, $PO_4^{3-}$). (**B**) Fluorescence photos of the **BAM-HM** probe before and after adding different anions. (**C**) Fluorescence spectra of different concentrations of $PO_4^{3-}$ were added to the solution of the **BAM-HM** probe. (**D**) Linear relationship between fluorescence intensity and $PO_4^{3-}$ concentration.

We observed that the complex showed a mole fraction with **BAM-HM** of 0.5 for $PO_4^{3-}$, which meant a 1:1 binding stoichiometry (Figure S12). Then, the sensitivity of the **BAM-HM** probe was studied using a titration experiment. As shown in Figure 2C, as the concentration of $PO_4^{3-}$ increased from 0 μM to 160 μM, the fluorescence intensity of the

**BAM-HM** probe at 500 nm increased gradually. The fluorescence intensity of the **BAM-HM** probe showed a good linear relationship with the $PO_4^{3-}$ concentration (Figure 2D), and the detection limit of **BAM-HM** was calculated to be 0.612 μM according to the formula LOD = 3σ/K [34–37].

### *2.4. Spectroscopic Response of Probe **BAM-HH** to $PO_4^{3-}$*

The fluorescent spectra responses of the **BAM-HH** probe toward various ions were studied using fluorescent spectra analytes. Only the introduction of $PO_4^{3-}$ led to an obvious green fluorescence enhancement (Figures 3A and S13). In addition, the addition of other anions and cations did not induce a significant fluorescence change (Figure 3B). The anti-interference experiment indicated that the presence of anions and cations caused a negligible impact on $PO_4^{3-}$ detection.

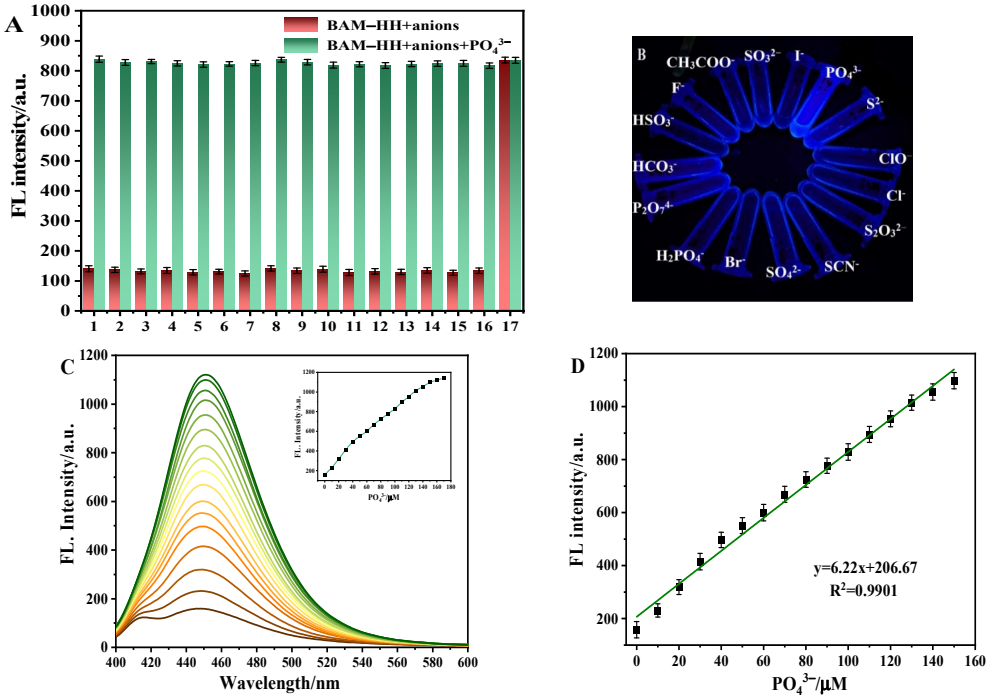



**Figure 3.** (**A**) Selectivity and interference of the **BAM-HH** probe for anions (1–16: $F^-$, $Cl^-$, $Br^-$, $I^-$, $HCO_3^-$, $CO_3^{2-}$, $AcO^-$, $SCN^-$, $SO_3^{2-}$, $ClO^-$, $HSO_3^-$, $SO_4^{2-}$, $S^{2-}$, $S_2O_3^{2-}$, $HPO_4^{2-}$, $PO_4^{3-}$). (**B**) Fluorescence photos of the **BAM-HH** probe before and after adding different anions. (**C**) Fluorescence spectra of different concentrations of $PO_4^{3-}$ were added to the solution of the **BAM-HH** probe. (**D**) Linear relationship between fluorescence intensity and $PO_4^{3-}$ concentration.

Subsequently, the binding stoichiometry of **BAM-HH** exhibited a 1:1 ratio for $PO_4^{3-}$ sensing (Figure S14). Then, fluorescence titrations for $PO_4^{3-}$ were performed in a DMF/$H_2O$ (5/5, *V*/*V*) solution. As shown in Figure 3C, with the addition of $PO_4^{3-}$ (0–170 μM), the maximum emission peak of the **BAM-HH** probe increased gradually, and the fluorescence intensities of the **BAM-HH** probe were linearly correlated with the $PO_4^{3-}$ concentrations (Figure 3D). The detection limit of **BAM-HH** was calculated to be 0.318 μM. These results suggested that **BAM-HM** and **BAM-HH** are highly sensitive toward $PO_4^{3-}$ [38–42] (Table S1).

### *2.5. Sensing Time and Stability Experiments*

To further elucidate the response time of the **BAM-HM** and **BAM-HH** probes to detect $PO_4^{3-}$, the fluorescence intensity of the **BAM-HM** and **BAM-HH** probes at different sensing times was recorded after adding $PO_4^{3-}$. With an increase in response time, the fluorescence intensity increased continuously. The fluorescence intensity of **BAM-HM** + $PO_4^{3-}$ at 500 nm reached its maximum value in 80 s and stayed almost unchanged at subsequent

times (Figure 4A). Meanwhile, after the addition of $PO_4^{3-}$, the **BAM-HH** probe also showed a shorter response time toward $PO_4^{3-}$ within 60 s (Figure 4B), which indicated that the **BAM-HM** and **BAM-HH** probe solutions could instantaneously determine $PO_4^{3-}$.

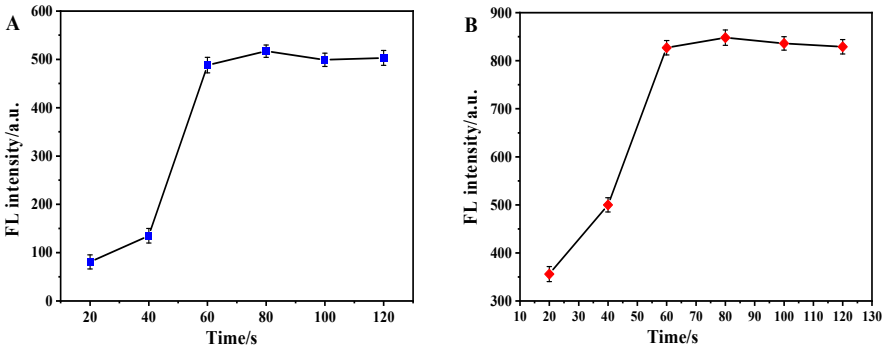



**Figure 4.** Fluorescence response time for the **BAM-HM** (**A**) and **BAM-HH** (**B**) probes with the addition of $PO_4^{3-}$.

Next, we studied the influence of the variation in pH values on the fluorescence performance of the **BAM-HM** and **BAM-HH** probes toward $PO_4^{3-}$. The fluorescent intensities of **BAM-HM** + $PO_4^{3-}$ (Figure S15A) and **BAM-HH** + $PO_4^{3-}$ (Figure S15B) increased in the range of pH 1–3 and showed good stability at diverse pH levels (from 4 to 11). These results suggest that **BAM-HM** and **BAM-HH** have the capability to identify $PO_4^{3-}$ at a wide range of pH levels.

### *2.6. Mechanism Studies*

To further investigate the sensing mechanisms of the two probes to $PO_4^{3-}$, $^1$H NMR and MS analyses in the presence of $PO_4^{3-}$ were performed. As shown in Figure 5A, the hydroxyl group (Ha) peak in the **BAM-HM** probe appeared at 5.91 ppm and disappeared upon complexation with $PO_4^{3-}$. Then, it was found that the hydroxyl group (Hb) of the **BAM-HH** probe at 9.87 ppm disappeared after $PO_4^{3-}$, which indicated that $PO_4^{3-}$ caused the deprotonation of the hydroxyl group (Figure 5C). The proposed mechanism is shown in Figure 5B, D. In addition, in the MS spectra of **BAM-HM** + $PO_4^{3-}$ and **BAM-HH** + $PO_4^{3-}$, a new peak at 439.2011 corresponding to **BAM-HM** + $PO_4^{3-}$ was observed (Figure S16A). According to Figure S16B, the peak at *m*/*z* 409.0913 supports the structure of **BAM-HH** + $PO_4^{3-}$. The above results further support the proposed mechanism.

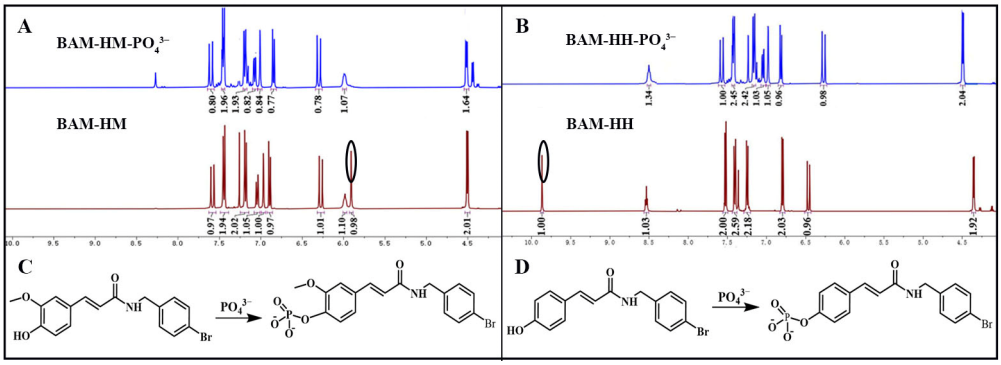



**Figure 5.** $^1$H NMR spectra of the **BAM-HM** (**A**) and **BAM-HH** (**C**) probes before and after adding $PO_4^{3-}$. The binding mechanism of the **BAM-HM** (**B**) and **BAM-HH** (**D**) probes.

The results of **BAM-HM**, **BAM-HM** + $PO_4^{3-}$, **BAM-HH,** and **BAM-HH** + $PO_4^{3-}$ are shown in Figure 6. In the **BAM-HM** probe, the HOMO and LUMO orbitals are mainly distributed on feruloyl, with an energy band gap of 4.1165 eV. The HOMO and LUMO orbitals of the **BAM-HH** probe are mainly distributed on 4-hydroxycinnamoyl, with the

energy level calculated at 4.3528 eV. A small amount of electron transfer in **BAM-HM** and **BAM-HH** led to weak fluorescence. From the calculation results, it could be seen that the LUMO of **BAM-HM** + $PO_4^{3-}$ was located in feruloyl, and the HOMO was distributed at the center of the $PO_4^{3-}$ ligand. In the **BAM-HH** + $PO_4^{3-}$, the electron clouds in the LUMO were distributed on the 4-hydroxycinnamoyl, and the HOMO was located at the $PO_4^{3-}$ center of **BAM-HH** + $PO_4^{3-}$. The energy gaps of **BAM-HM** + $PO_4^{3-}$ and **BAM-HH** + $PO_4^{3-}$ were 3.380 eV and 3.460 eV, respectively. The energy gaps of **BAM-HM** + $PO_4^{3-}$ and **BAM-HH** + $PO_4^{3-}$ were smaller than those of **BAM-HM** and **BAM-HH**, suggesting that **BAM-HM** and **BAM-HH** tend to bind $PO_4^{3-}$, and the combined complex is more stable. The energy gap of **BAM-HM** + $PO_4^{3-}$ was smaller than that of **BAM-HH** + $PO_4^{3-}$, indicating that the intramolecular charge transfer (ICT) process of **BAM-HH** + $PO_4^{3-}$ was weakened compared with that of **BAM-HM** + $PO_4^{3-}$. The above results were consistent with the experimental results.

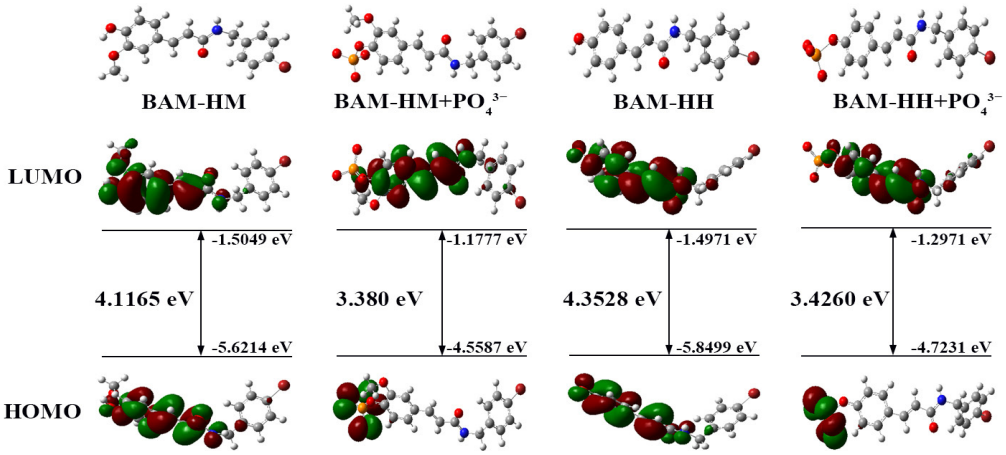



**Figure 6.** Frontier molecular orbital profiles of **BAM-HM**, **BAM-HH**, **BAM-HM** + $PO_4^{3-}$, and **BAM-HH** + $PO_4^{3-}$.

### *2.7. Application in Real Water Samples*

Next, the practical application of the two probes was investigated, and we estimated the $PO_4^{3-}$ concentration in water samples via two probes. Different concentrations of $PO_4^{3-}$ were added to water samples. First, the fluorescence intensity of **BAM-HM** and **BAM-HH** mixed with different $PO_4^{3-}$ concentrations (2, 5, 10, and 15 μM) was recorded. The corresponding recoveries are shown in Tables S2 and S3. The recovery rate for $PO_4^{3-}$ ranged from 96 to 105%, indicating that **BAM-HM** and **BAM-HH** have the ability to evaluate the level of $PO_4^{3-}$ in real water samples.

### *2.8. Cell Imaging*

Prior to the fluorescence imaging experiment, the toxicity of the **BAM-HM** and **BAM-HH** probes in HeLa cells was studied using the CCK8-assay. HeLa cells were treated with different concentrations (0–200 μM) of the two compounds for 24 h. As shown in Figure S17, the cell survival ratios of the two compounds were above 80% at a concentration of 100 μM. These results suggested that **BAM-HM** and **BAM-HH** showed low cytotoxicity and could be used for cell imaging experiments.

Then, the capacity of the **BAM-HM** and **BAM-HH** probes was examined in HeLa cells. As displayed in Figure 7A, when the cells were incubated with the **BAM-HM** probe, no obvious fluorescence was observed. Then, the pre-treated cells were treated with different concentrations of $PO_4^{3-}$ (0, 5 μM, 10 μM, 15 μM, and 20 μM), and a faint green fluorescence was observed; the intracellular green fluorescence was clearly enhanced with an increase in $PO_4^{3-}$ concentration. In addition, the HeLa cells were incubated with the **BAM-HH** probe, which showed weak fluorescence. The **BAM-HH**-loaded HeLa cells were further treated with different concentrations of $PO_4^{3-}$ (0, 5 μM, 10 μM, 15 μM, and 20 μM). With

an increase in $PO_4^{3-}$ concentration, an obvious fluorescence enhancement in the blue channel was observed (Figure 7B). The cell experiments demonstrate that the **BAM-HM** and **BAM-HH** probes can be potentially used as a powerful tool for the detection of $PO_4^{3-}$ in vivo.

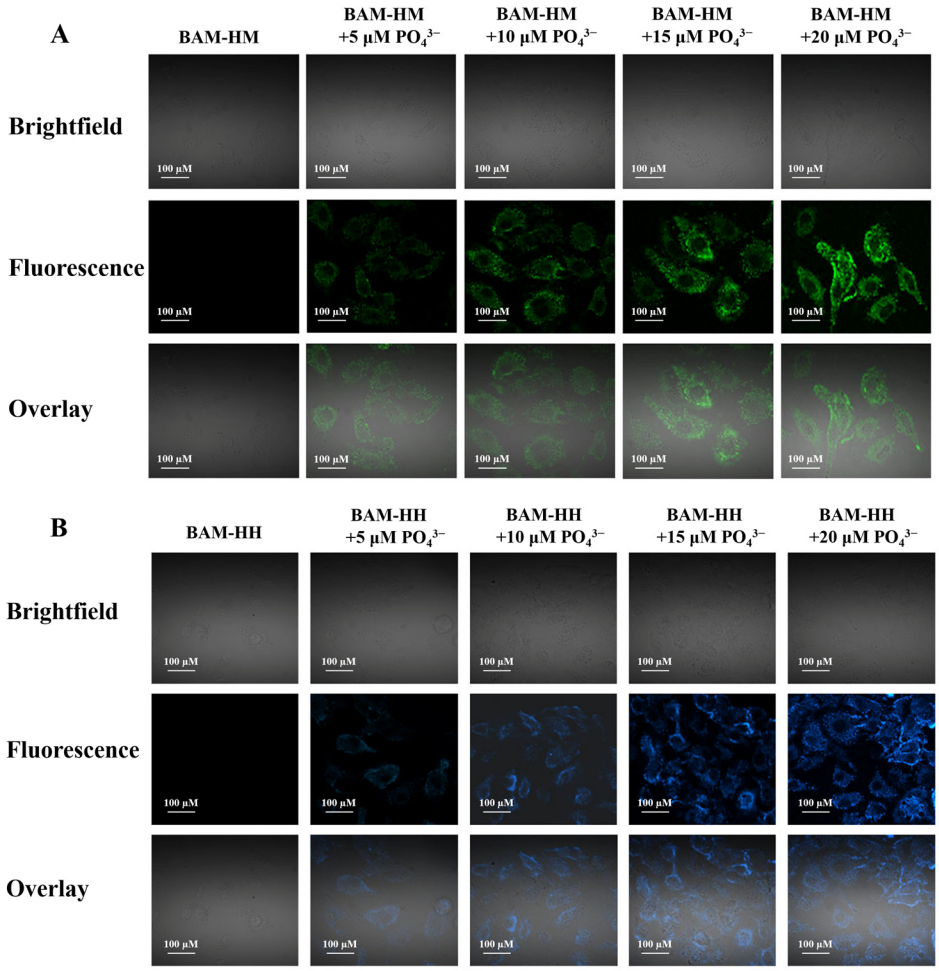



**Figure 7.** The fluorescence imaging of HeLa cells treated with the **BAM-HM** (**A**) and **BAM-HH** (**B**) probes and then incubated with different concentrations of $PO_4^{3-}$ (5 μM, 10 μM, 15 μM, and 20 μM).

## 3. Materials and Methods

### *3.1. General Instrumentations and Reagents*

The chemicals and solvents in this study were purchased from chemical suppliers (Titan, shanghai, China) and used as received without further purification. Compounds were characterized by $^1H$ and $^{13}C$ NMR spectra (Bruker, Billerica, MA, USA) and ESI-MS (Agilent, Santa Clara, CA, USA). The fluorescence spectrum of the probe was recorded using a fluorescence spectrometer (Hitachi, Kyoto, Japan). The pH measurements were recorded by a pH measuring apparatus (Ohaus, NJ, USA). The purity of the compounds was recorded using an LCMS spectrometer (Agilent, CA, USA). The fluorescence cell imaging was performed using a confocal laser scanning microscope (Leica, Wetzlar, Germany).

### *3.2. General Synthetic Procedure for **BAM-HM**, **BAM-MM**, and **BAM-HH***

**BAM-HM**: 4-hydroxy-3-methoxycinnamic acid (138.52 mg, 0.7 mmol), 1-Ethyl-3-(3-dimethylaminopropyl) carbodiimide (EDCl, 134.90 mg, 0.7 mmol) and 1-Hydroxybenzotriazole (HOBT, 95.71 mg, 0.7 mmol) were mixed with 20 mL of DMF. After 20 min, 4-bromobenzylamine (259.81 mg, 1.4 mmol) was added and stirred for another 20 min at room temperature. Then N, N-Diisopropylethylamine (180.36 mg, 1.4 mmol) was added to the

aforesaid solution and stirred for 24 h. After the reaction was completed, the mixture was extracted with ethyl acetate, and the residue was obtained after the solvent was removed. Then, the residue was purified using silica gel column chromatography (PE/EA = 5/1) to yield the product, which was a pale yellow solid (93.22 mg, 68.6%). $^{1}$H NMR (400 MHz, $CDCl_3$-$d_6$) δ 7.58 (d, *J* = 15.5 Hz, 1H), 7.49–7.39 (m, 2H), 7.25–7.15 (m, 2H), 7.04 (dd, *J* = 8.2, 2.0 Hz, 1H), 6.97 (d, *J* = 1.9 Hz, 1H), 6.89 (d, *J* = 8.2 Hz, 1H), 6.28 (d, *J* = 15.6 Hz, 1H), 5.98 (s, 1H), 5.91 (s, 1H), 4.51 (d, *J* = 5.9 Hz, 2H), 3.89 (s, 3H). $^{13}$C NMR (126 MHz, DMSO-$d_6$) δ 165.48, 148.36, 147.81, 139.51, 139.14, 131.15, 129.51, 126.29, 121.59, 119.74, 118.57, 115.65, 110.82, 55.51, 41.61. ESI-MS *m*/*z*: $[M + H]^+$ calculated for $C_{17}H_{16}BrNO_3$ 362.0215, found 362.0589.

**BAM-MM**: **BAM-MM** was prepared using 3,4-dimethoxycinnamic acid (124 mg, 0.6 mmol) instead of 4-hydroxy-3-methoxycinnamic acid, according to a similar procedure for **BAM-HM**. The product was a yellow solid (164.71 mg, 73.2%). $^{1}$H NMR (400 MHz, $CDCl_3$-$d_6$) δ 7.60 (d, *J* = 15.5 Hz, 1H), 7.45 (dd, *J* = 8.5, 2.6 Hz, 2H), 7.21–7.17 (m, 2H), 7.07 (dd, *J* = 8.3, 2.1 Hz, 1H), 7.01 (d, *J* = 2.0 Hz, 1H), 6.85 (d, *J* = 8.3 Hz, 1H), 6.30 (d, *J* = 15.5 Hz, 1H), 5.99 (s, 1H), 4.51 (d, *J* = 5.8 Hz, 2H), 3.89 (d, *J* = 5.9 Hz, 6H). $^{13}$C NMR (126 MHz, DMSO-$d_6$) δ 165.33, 150.14, 148.88, 139.16, 139.08, 131.15, 129.52, 127.60, 121.40, 119.76, 119.58, 111.73, 110.01, 55.53, 55.40, 41.63. ESI-MS *m*/*z*: $[M + H]^+$ calculated for $C_{18}H_{18}BrNO_3$ 376.2604, found 376.2741

**BAM-HH**: **BAM-HH** was prepared using 4-hydroxycinnamic acid (98.43 mg, 0.6 mmol) instead of 4-hydroxy-3-methoxycinnamic acid, according to a similar procedure for **BAM-HM**. The product was a yellow solid (139.42 mg, 70.2%). $^{1}$H NMR (500 MHz, DMSO-$d_6$) δ 9.87 (s, 1H), 8.53 (t, *J* = 6.1 Hz, 1H), 7.56–7.49 (m, 2H), 7.44–7.38 (m, 3H), 7.29–7.20 (m, 2H), 6.83–6.76 (m, 2H), 6.46 (d, *J* = 15.7 Hz, 1H), 4.35 (d, *J* = 6.0 Hz, 2H). $^{13}$C NMR (126 MHz, DMSO-$d_6$) δ 165.95, 159.39, 139.70, 139.62, 131.63, 130.01, 129.74, 126.28, 120.22, 118.74, 116.22, 42.08. ESI-MS *m*/*z*: $[M + H]^+$ calculated for $C_{16}H_{14}BrNO_2$ 332.9208, found 332.9353.

### *3.3. General Protocol Photophysical Properties Experiments*

The stock solutions of the **BAM-HM** and **BAM-HH** probes (1 mM) were prepared in a DMF solution ($V_{DMF}/V_{H2O}$ = 1/1, pH = 7), and the test solutions were diluted to a concentration of 10 μM. In the pH and time response experiments, the concentrations of the two probes were maintained at 10 μM, and the test system with various pH levels was adjusted with HCl and NaOH solutions. In the sensitivity experiments, different concentrations of $PO_4^{3-}$ were added to the solutions of the probes (10 μM). Furthermore, in the selectivity experiments, different anions ($I^-$, $F^-$, $Br^-$, $Cl^-$, $AcO^-$, $HCO_3^-$, $CO_3^{2-}$, $SCN^-$, $SO_3^{2-}$, $HSO_3^-$, $ClO^-$, $SO_4^{2-}$, $S_2O_3^{2-}$, $S^{2-}$, $PO_4^{3-}$, and $HPO_4^{2-}$) and cations ($Cr^{3+}$, $Co^{2+}$, $Cd^{2+}$, $Cu^{2+}$, $Ba^{2+}$, $Ni^{2+}$, $Ag^+$, $Al^{3+}$, $Zn^{2+}$, $Hg^{2+}$, $Na^+$, $Mg^{2+}$, $Mn^{2+}$, $Fe^{2+}$, and $Fe^{3+}$) were dissolved in deionized water, and the concentration of anions and cations was maintained at 100 μM. All fluorescence measurements were investigated in ($V_{DMF}/V_{H2O}$ = 1/1, pH = 7) at room temperature, the optimal excitation wavelength was set to 350 nm, and the excitation and emission slit widths were set to 10 nm and 10 nm.

### *3.4. Cytotoxicity and Cell Imaging Experiments*

The cytotoxicity of the **BAM-HM** and **BAM-HH** probes was estimated with the CCK8-assay [43–46]. HeLa cells were cultured in an RPMI-1640 medium containing 10% FBS and 1% antibiotics. Then, treated HeLa cells were further incubated with the two different probe solutions (3.13, 6.25, 12.5, 25, 50, 100, and 200 μM) for 24 h. Afterward, each well of plates was further injected with the CCK-8 solution. Four hours later, according to the optical density of the experimental group, the cell viability was determined.

HeLa cells were cultured in an RPMI-1640 medium containing a 10 μM probe solution for 1 h. For cell fluorescence imaging, the probe-pretreated cells were then treated with 5, 10 μM, 15 μM, and 20 μM $PO_4^{3-}$ for 30 min, respectively. After washing three times with HEPES (2-[4-(2-hydroxyethyl)piperazin-1-yl]ethanesulfonic acid) buffer, the HeLa cells

were utilized for cell imaging. Finally, fluorescent photographs of the cells were acquired using a confocal fluorescence microscope.

## 4. Conclusions

In conclusion, we successfully prepared two fluorescence probes (**BAM-HM** and **BAM-HH**) based on a caffeic acid derivative for the detection of $PO_4^{3-}$. In particular, the two probes can detect $PO_4^{3-}$ with an obvious fluorescence enhancement in the green channel (**BAM-HM**) and blue channel (**BAM-HH**), respectively. The two probes have multiple advantages, such as good sensitivity (**BAM-HM**, 0.612 μM; **BAM-HH**, 0.318 μM) and selectivity, a wide range of pH applications (3–11), short reaction times (**BAM-HM**, 80 s; **BAM-HH**, 60 s), and low cytotoxicity. The quantitative determination of $PO_4^{3-}$ in real water samples was investigated. Additionally, the applications of two probes in cell imaging $PO_4^{3-}$ were demonstrated. Therefore, this study provides an efficient analytical method for the detection and monitoring of $PO_4^{3-}$ in ecological environments and in vivo.

**Supplementary Materials:** The following supporting information can be downloaded at: https://www.mdpi.com/article/10.3390/ijms252111680/s1.

**Author Contributions:** Conceptualization, P.Z. and Q.J.; methodology, X.Z. and Q.J.; data curation, methodology; software, X.Z., X.R. and Y.Z.; funding acquisition, Q.J. and X.Y.; writing—original draft preparation, X.Z.; writing—review and editing, Q.J. All authors have read and agreed to the published version of the manuscript.

**Funding:** This research was funded by the National Natural Science Foundation of China (No. 32160350), Yunnan Fundamental Research Projects (No. 202201AU070069, 202301BD070001-117).

**Institutional Review Board Statement:** Not applicable.

**Informed Consent Statement:** Not applicable.

**Data Availability Statement:** Supplementary Materials: Available: $^{1}H$ and $^{13}C$ NMR spectra and HRMS spectra of **BAM-HM**, **BAM-HH,** and **BAM-MM**.

**Conflicts of Interest:** The authors declare no conflicts of interest.

## References

1. Huang, L.X.; Bai, H.Y.; Tao, H.; Cao, Q.Y. Cleft-type imidazoliums for sensing of sulfate and polyphosphate anions with AIE emission. *Dyes Pigm.* **2020**, *181*, 108553. [CrossRef]
2. Farahani, S.M.; Dadmehr, M.; Karimi, M.A.; Korouzhdehi, B.; Karimi, M.A.; Rajabian, M. Fluorometric detection of phytase enzyme activity and phosphate ion based on gelatin supported silver nanoclusters. *Food Chem.* **2022**, *396*, 133711. [CrossRef] [PubMed]
3. Choudhary, V.; Philip, L. Stable paper-based colorimetric sensor for selective detection of phosphate ion in aqueous phase. *Microchem. J.* **2021**, *171*, 106809. [CrossRef]
4. Chen, B.B.; Li, R.S.; Liu, M.L.; Zou, H.Y.; Hui, L.; Huang, C.Z. Highly selective detection of phosphate ion based on a single-layered graphene quantum dots-$Al^{3+}$ strategy. *Talanta* **2018**, *178*, 172–177. [CrossRef] [PubMed]
5. Hazarika, G.; Das, S.; Das, N.M.; Manna, D. A pH-responsive covalent organic network: Morphology change leads to capture and removal of phosphate ions from water. *J. Mater. Chem. A* **2024**, *12*, 19559–19566. [CrossRef]
6. Zhang, R.; Jiang, L.H.; Duan, N.; Fu, W.S.; Ma, J.; Sun, X.L.; Liao, J.Q.; Jin, H. High-accuracy quantitative model for phosphate anions in solution based on absorption spectroscopy and machine learning algorithms. *J. Clean. Prod.* **2024**, *467*, 142871. [CrossRef]
7. Chourasia, J.; Tohora, N.; Mahato, M.; Sultana, T. A sulfone-based fluorogenic probe for cascade detection of $Zn^{2+}$ and $PO_4^{3-}$ ions. *J. Mol. Struct.* **2024**, *1304*, 137736. [CrossRef]
8. Patella, B.; Parisi, A.; Moukri, N.; Gitto, F.; Russo, M.; Inguanta, R. Phosphate ions detection by using an electrochemical sensor based on laser-scribed graphene oxide on paper. *Electrochim. Acta* **2023**, *461*, 142600. [CrossRef]
9. Mokrzycki, J.; Fedyna, M.; Marzec, M.; Klimek, A.; Bajda, T.; Hersztek, M.M. Copper ion-exchanged zeolite X from fly ash as an efficient adsorbent of phosphate ions from aqueous solutions. *J. Environ. Chem. Eng.* **2022**, *10*, 108567. [CrossRef]
10. Manyatshe, A.; Balogun, M.O.; Nkambule, T.T.I.; Msagati, T.A.M. Chitosan modified sugarcane bagasse biochar for the adsorption of inorganic phosphate ions from aqueous solution. *J. Environ. Chem. Eng.* **2022**, *10*, 108243. [CrossRef]
11. Zhang, X.P.; Wang, J.J.; Juan, Y.; Yang, H.; Wei, W.; Zhao, J. A novel fluorescence method for detection of phosphate anions based on porphyrin metalation. *Spectrochim. Acta A* **2022**, *274*, 121136. [CrossRef] [PubMed]

12. Semen, S.; Mercan, S.; Yayla, M.; Açıkkol, M. Elemental composition of green coffee and its contribution to dietary intake. *Food Chem.* **2017**, *215*, 92–100. [CrossRef] [PubMed]
13. Hutchinson, R.W.; Cox, A.G.; Howlett, D.R. Imaging and spatial distribution of beta-amyloid peptide and metal ions in Alzheimer's plaques by laser ablation-inductively coupled plasma-mass spectrometry. *Anal. Biochem.* **2005**, *346*, 225–233. [CrossRef] [PubMed]
14. Dravecz, G.; Bencs, L.; Beke, D.; Gali, A. Determination of silicon and aluminum in silicon carbide nanocrystals by high-resolution continuum source graphite furnace atomic absorption spectrometry. *Talanta* **2016**, *147*, 271–275. [CrossRef]
15. Smith, C.D.; Dietz, M.L. Support loading effects on the performance of an extraction chromatographic resin: Toward improved separation of trivalent lanthanides. *Talanta* **2021**, *222*, 121541. [CrossRef] [PubMed]
16. Song, J.X.; Chen, P.F.; Zhang, L.S.; Hu, J.B.; Yang, R.N.; Lu, X.M.; Fan, Q.L. A novel near-infrared-II fluorescence probe for serum albumin biosensing and site-binding mechanism study. *Sens. Actuators B Chem.* **2024**, *418*, 136355. [CrossRef]
17. Xue, H.; Lu, J.; Zhang, X.; Guo, L. γ-Glutamyl transpeptidase–activated indole-quinolinium based cyanine as a fluorescence turn-on nucleolus-targeting probe for cancer cell detection and inhibition. *Talanta* **2022**, *237*, 122898. [CrossRef]
18. Du, L.; Xie, Y.Q.; Sun, X.Y.; Wang, L. A new coumarin-based "turn-on" fluorescence probe with high sensitivity and specificity for detecting hypochlorite ion. *Dyes Pigm.* **2022**, *200*, 110137–110143. [CrossRef]
19. Ma, J.Y.; Kong, X.T.; Zhao, M.T.; Jiao, Z.L.; Li, H.; Zhang, Z.X. A dual-functional NIR fluorescence probe for detecting hypochlorous acid and bisulfite in biosystem. *Anal. Chim. Acta* **2024**, *1320*, 342993. [CrossRef]
20. Walter, E.R.H.; Lee, L.C.C.; Leung, P.K.K.; Lo, K.K.W.; Long, N.J. Mitochondria-targeting biocompatible fluorescent BODIPY probes. *Chem. Sci.* **2024**, *15*, 4846. [CrossRef]
21. Wang, X.; Ding, Q.; Wu, L.L.; Mao, Y.T.; Che, F.; Kotova, O.; Li, P.; Tang, B. Mitochondria-targeting biocompatible fluorescent BODIPY probes. *Chem. Rev.* **2024**, *124*, 7106–7164. [CrossRef] [PubMed]
22. Zhang, C.; Wu, G.Z. Recent advances in fluorescent probes for ATP imaging. *Talanta* **2024**, *279*, 126622. [CrossRef] [PubMed]
23. Sharma, A.; Verwilst, P.; Li, M.; Ma, D.; Singh, N.; Yoo, J.; Kim, Y.; Kim, S. Theranostic fluorescent probes. *Chem. Rev.* **2024**, *124*, 2699–2804. [CrossRef] [PubMed]
24. Li, X.X.; Ma, C.Y.; Du, M.X.; Dong, W.K.; Ding, Y.J. A rare salamo-salophen type "on-off-on" fluorescent probe for relay recognition of $Hg^{2+}$ and phosphate ions and its applications. *J. Mol. Struct.* **2024**, *1299*, 137188. [CrossRef]
25. Maiti, A.; Tohora, N.; Roy, D.; Ray, T. A symmetrical imine-linkage colorimetric probe for sequential detection of $Al^{3+}$ and $PO_4^{3-}$ ions. *Inorg. Chim. Acta* **2024**, *564*, 121966. [CrossRef]
26. Dai, Y.P.; Wang, P.; Fu, J.X.; Yao, K.; Xu, K.X. A quinoline-based $Cu^{2+}$ ion complex fluorescence probe for selective detection of inorganic phosphate anion in aqueous solution and its application to living cells. *Spectrochim. Acta A* **2017**, *183*, 30–36. [CrossRef]
27. Das, S.; Das, P.P.; Walton, J.W. An excited state intramolecular proton transfer induced phosphate ion targeted ratiometric fluorescent switch to monitor phosphate ions in human peripheral blood mononuclear cells. *Dalton Trans.* **2022**, *51*, 10779. [CrossRef]
28. Kaur, I.; Kaur, P.; Singh, K. 2-(4-Amino-2-hydroxyphenyl) benzothiazole based Schiff-base: Complexation/decomplexation driven photo physical tuning of fluorescence leading to $Cu^{2+}$ and $PO_4^{3-}$ detection. *Sens. Actuators B Chem.* **2018**, *257*, 1083–1092. [CrossRef]
29. Kadar, N.N.M.A.; Teoh, S.L.; Yahaya, M.F. Caffeic acid on metabolic syndrome: A review. *Molecules* **2021**, *16*, 5490. [CrossRef] [PubMed]
30. Meinhart, A.D.; Wagner, R.; Godoy, H.T. Chlorogenic and caffeic acids in 64 fruits consumed in Brazil. *Food Chem.* **2019**, *286*, 51–63. [CrossRef]
31. Masuda, T.; Fukuyama, Y.Y.; Kurosawa, S.; Fujii, S. Effects of temperature on the composition and xanthine oxidase inhibitory activities of caffeic acid roasting products. *J. Agric. Food Chem.* **2019**, *32*, 8977–8985. [CrossRef] [PubMed]
32. Qin, J.J.; Yang, M.; Wa, W.Q.; Zheng, J. Interaction between caffeic acid/caffeic acid phenethyl ester and micellar casein. *Food Chem.* **2021**, *349*, 129154–129160. [CrossRef] [PubMed]
33. Song, J.; Yang, X.Q.; Xie, S.D.; Rao, X.P.; Zhao, P.; Jiang, Q. A novel "turn on" fluorescence probe based on a caffeic acid skeleton for detecting $Al^{3+}$ and bioimaging application. *Anal. Methods* **2023**, *15*, 3233. [CrossRef] [PubMed]
34. Qiang, J.; Han, Z.F.; Guo, Z.W.; Wang, Y.R.; Li, Y.J.; Wang, F.; Chen, X.Q. A novel "AND" logic platform based on ICT and FRET for constructing near-infrared dual-locked fluorescence probe. *Dyes Pigm.* **2024**, *229*, 112292. [CrossRef]
35. Ma, J.Y.; Kong, X.T.; Wang, X.S.; Zhao, M.T.; Xie, H.; Jiao, Z.L.; Zhang, Z.X. A dual-oxidant sensing fluorescence probe for detecting hydroxyl radicals and hypochlorous acid in living cells and zebrafish. *Sens. Actuators B Chem.* **2024**, *417*, 136209. [CrossRef]
36. Ou, Z.Q.; Wang, M.X.; Zhang, Z.Y.; Liang, J.Q.; Tang, J.W.; Ma, L.J. A fluorescence and colorimetric bifunctional probe for recognition of $Al^{3+}$ and $Cu^{2+}$ and its applications in cells and environmental water systems. *Microchem. J.* **2023**, *195*, 109386. [CrossRef]
37. Meng, Y.; Liu, C.; Ding, H.; Yao, P.Y.; He, S.; Zeng, X.S. A novel tethered phenothiazine-coumarin fluorescence probe for rapid detection of hypochlorite ion and its applications. *Dyes Pigm.* **2023**, *218*, 111470. [CrossRef]
38. Tang, X.; Wang, Y.; Han, J.; Ni, L.; Wang, L. A relay identification fluorescence probe for $Fe^{3+}$ and phosphate anion and its applications. *Spectrochim. Acta A* **2018**, *191*, 172–179. [CrossRef]

39. Mahto, B.; Chand, S.; Singh, D.V.; Patra, S.; Chandra, G. Synthesis of hybrid azobenzene-chalcone dyes and studies on their photophysical properties: Molecular recognition of carbonate and phosphate ions using a novel turn-off fluorescent probe. *J. Mol. Struct.* **2024**, *1306*, 137839. [CrossRef]
40. Liu, R.J.; Tang, X.; Wang, Y.; Han, J.; Zhang, H.Q. A fluorescent chemosensor for relay recognition of $Fe^{3+}$ and $PO_4^{3-}$ in aqueous solution and its applications. *Tetrahedron* **2017**, *73*, 5229–5238. [CrossRef]
41. Jiang, X.J.; Fu, Y.; Xu, L.H.; Lu, H.L. A novel acridine-based fluorescent probe for the cascade recognition of $Cr^{3+}$ and $PO_4^{3-}$. *Sens. Actuators B Chem.* **2014**, *202*, 388–394. [CrossRef]
42. Sultana, T.; Mahato, M.; Tohora, N.; Ahamed, S. An azine-based chromogenic, fluorogenic probe for specific cascade detection of $Al^{3+}$ and $PO_4^{3-}$ ions. *J. Photoch. Photobio. A* **2013**, *444*, 114951. [CrossRef]
43. Jiang, L.H.; Cai, X.L.; Li, S.; Miao, Y.; Chen, L.; He, X.Z.; Weng, Z.Q. Hydroxyethyl starch curcumin enhances antiproliferative effect of curcumin against HepG2 Cells via apoptosis and autophagy induction. *Front. Pharmacol.* **2021**, *12*, 755054. [CrossRef] [PubMed]
44. Zhao, R.; Shen, Y.B.; Zhao, C.Y.; Wu, C.F.; Liu, Y.Y.; Lu, Z.T. A rapid screening platform for antibiotic susceptibility testing based on a simple colorimetric method. *Analyst* **2023**, *148*, 4148–4155. [CrossRef] [PubMed]
45. Wu, F.F.; Wu, Z.W.; Wang, X.Y.; Liu, Y.L.; Ye, Q. High-precision detection of cellular drug response based on SERS spectrum and multivariate statistical analysis. *Biosensors* **2023**, *13*, 241. [CrossRef]
46. Wang, T.K.; Xu, S.T.; Fan, Y.J.; Wu, J.; Chen, Y.; Zhang, Y.J. The Synergistic effect of proanthocyanidin and HDAC inhibitor inhibit breast cancer cell growth and promote apoptosis. *Int. J. Mol. Sci.* **2023**, *24*, 10476. [CrossRef]


**Disclaimer/Publisher's Note:** The statements, opinions and data contained in all publications are solely those of the individual author(s) and contributor(s) and not of MDPI and/or the editor(s). MDPI and/or the editor(s) disclaim responsibility for any injury to people or property resulting from any ideas, methods, instructions or products referred to in the content.